Electromagnetic conductivity and GPR surveys across a Prototype Surface Barrier to Determine Variations in Soil Moisture Content

Final Report for Task Order 407099-A-B3

William P. Clement

Center for Geophysical Investigation of the Shallow Subsurface

Boise State University

Boise, ID 83725

CGISS Technical Report 02-05

Electromagnetic conductivity and GPR surveys across a Prototype Surface Barrier to Determine Variations in Soil Moisture Content

Final Report for Task Order 407099-A-B3

William P. Clement

Center for Geophysical Investigation of the Shallow Subsurface

Boise State University

Boise, ID 83725

Abstract

Surface barriers covering landfills must ensure that water does not flow through the landfill. Knowing the amount of water and the changes in water content over time will allow engineers to monitor the effectiveness of the surface barriers. To measure changes in soil moisture content, I collected electromagnetic induction and GPR data. I compared the changes in electromagnetic conductivity and GPR response over a one year period. Since the thickness and the composition of the prototype surface barrier did not change over this time, differences in the electromagnetic response are due to changes in soil moisture or water content in the barrier. GPR images changes in the subsurface that indicate changes in soil moisture content. My results confirm that the prototype surface barrier is drier the Summer and wetter in the Winter.

Introduction

Understanding fluid flow in the unsaturated zone has an important role in determining the fate and transport of contaminants. The distribution of hydraulic conductivity is vital to accurate models of vadose zone fluid flow. A reliable and non-invasive method to determine the hydraulic conductivity is desired to adequately map the hydraulic conductivity distribution in surface barriers. The hydraulic conductivity distribution will provide better input to fate and transport modeling packages and thus increase the reliability of the resulting models.

At Hanford, prototype surface barriers are being tested to determine their ability to protect contaminants from through-flowing fluids (200-BP-1, 1999). The surface barrier (figure 1) is
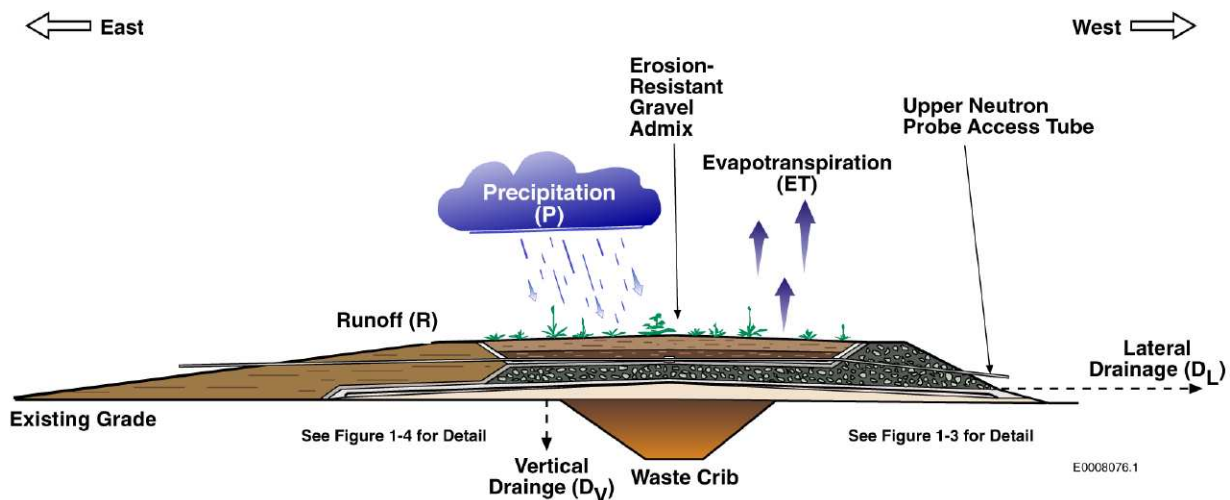
Figure 1. Cutaway diagram of the prototype surface barrier showing the construction and thicknesses of various materials. The hydrological cycle is also described in the figure.

engineered to reduce the fluid flow through the underlying waste crib. The upper 2 m of the surface barrier consist of two, 1.0 m thick layers of silt loam, a 0.15 m sand filter, and a 0.3 m thick gravel filter underlain by asphalt. I was contracted to use non-invasive geophysical methods to

determine the spatial distribution and the seasonal changes in the soil moisture content in this upper ~ 2.5 m zone above the asphalt.

Measurement of the electromagnetic (EM) properties of the subsurface can provide estimates of important hydrological parameters such as porosity and water saturation. In turn, these properties are used by hydrologists and soil scientists to determine the hydraulic conductivity of the saturated and unsaturated zones using relationships like Richards equation and the van Genuchten parameters (van Genuchten, 1980). Importantly, EM methods are deployed across the ground surface and are thus a non-invasive method to sample the subsurface. EM methods such as electromagnetic induction and ground penetrating radar (GPR) acquire data quickly and at high spatial densities to provide a detailed distribution of EM conductivity or velocity.

Sheets and Hendrickx (1995) used electromagnetic induction to determine the soil moisture content. The electrical conductivity of soil can indirectly map changes in the water content (Curtis, 2001; Davis et al., 1997; McNeill, 1980a). Although other factors, such as mineralogy, effect the EM conductivity, at the landfill site the material is fairly homogeneous. Thus, variations in the EM conductivity may be correlated to variations in soil moisture content.

Many experiments have used GPR to test the validity of using radar energy to map soil moisture content (Berktold et al., 1998; Chanzy et al., 1996; Charlton, 2000; Du and Rummel, 1994:, Greaves et al., 1996; Huisman et al., 2001; Lesmes et al., 1999; van Overmeeren et al., 1997; Weiler et al., 1998). Most of these experiments were small, test-of-concept surveys. Grote et al. (2002) have used GPR to monitor the volumetric water content in soils applied to highway construction and maintenance. Hubbard et al. (2002) have recently used GPR to map soil moisture content across a vineyard. GPR measurements are converted to soil moisture content and have shown promising results for measuring soil moisture content.

Methods

EM31 surveys

Electromagnetic induction surveys provide a three-dimensional distribution of the conductivity of the subsurface. Electrical conductivity is a measure of the ease of flow of electrons through a material. Metals and ionic solutions, such as saline water, have a high conductivity. Silicate minerals tend to have a low conductivity. A widely used tool for measuring EM ground conductivity is the Geonics EM31 instrument. The EM31 instrument uses a dipole-dipole loop and operates at 9.8 KHz. The loop separation is 3.66 m resulting in a sampling depth of about 6.0 m (McNeill, 1980b). The dipoles can be oriented vertically or horizontally. The EM31 acquires the quadrature and in-phase components of the magnetic field. The quadrature component measures the ground conductivity (in mS/m). The in-phase component, the ratio of the secondary to the primary magnetic field (in parts per thousand), is more sensitive to large metallic objects than the quadrature component.

The EM conductivity changes can be related to soil water content (Curtis, 2001; Davis et al., 1997; McNeill, 1980a). The electrical conductivity of soils depends on the porosity and the percent of moisture in the pores (McNeill, 1980a). At the surface barrier, the geological setting is essentially constant, so changes in electrical conductivity are most likely caused by changes in the soil moisture content. Thus, by mapping the electrical conductivity, I am also indicating changes in the soil moisture content.

GPR surveys

GPR sends radar energy into the ground through a transmitting antenna. This energy is recorded at a receiving antenna placed near the transmitter. For the data used in this study, 100 MHz antennas were used. A few 200 MHz surveys were conducted, but the data quality was too poor to reliably determine the arrivals. The sample interval was 0.8 ns and 500 samples were

4

acquired for each trace for a recording window of 400 ns. I stacked the data 64 times for the March data, 32 times for the rest of the data. The reduced number of stacks did not deteriorate the data quality and increased the acquisition rate.

Figure 2 shows the transmitter and receiver antennas and a simplified sketch of the arriv-
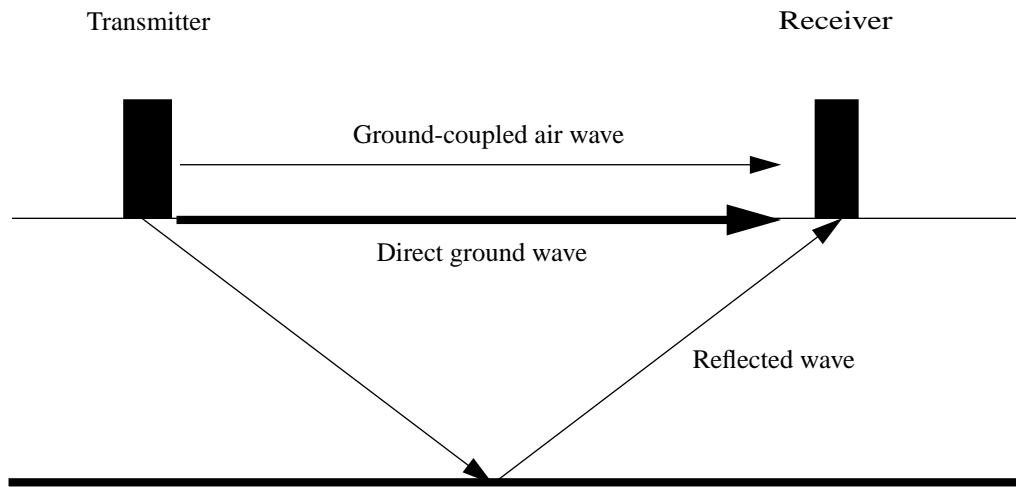
Figure 2. Arrivals recorded in the wide offset reflection profiles. The direct ground wave and reflection can provide estimates of the EM velocity of the surface between the antennas.

ing phases. The ground-coupled air wave travels directly between the transmitter and the receiver. This phase is the first arrival and has an EM velocity of air, 0.3 m/ns. The direct ground wave travels along the ground surface. The EM velocity from this phase corresponds to the EM velocity of the ground. The reflected arrival travels from the transmitter to an interface then is reflected back to the surface where the receiver records the energy.

The EM velocity of the phase is determined from the travel times. Water has a slow EM velocity (0.033 m/ns) and air has a fast EM velocity (0.3 m/ns). In most surveys, the material does not change in terms of composition or structure over time. Slower velocities indicate a higher

amount of water in the pore space. Thus, changes in EM velocity at the prototype surface barrier are caused by changing soil moisture.

The method indirectly measures the dielectric constant of the material through which the energy propagates. The dielectric constant or dielectric permittivity measures the ability of a material to polarize or store energy through separation of bound charges. Water has a high dielectric constant of about 80. Air has a dielectric constant of 1. Dry soil materials and sediments have dielectric constants between 3 and 10. Clays and silts may have a dielectric constant as high as about 30 to 40. The large dielectric constant difference between water and air enables mapping of changes in water content across a survey.

I conducted GPR surveys using two approaches to determine the EM velocity of the subsurface. The first method is the traditional common midpoint (CMP) method. The second method involves studying changes in the arrival time of known radar events and then converting this time to EM velocity (figure 4.) (Du and Rummel, 1994; Berktold et al., 1998). This second method is not widely applied in GPR surveys, but offers great potential to provide spatially densely sampled EM velocity measurements that can be converted to the desired parameters, such as dielectric constant or soil moisture content.

CMP geometry

Figure 3 shows the acquisition geometry of a CMP gather. CMPs are acquired by moving
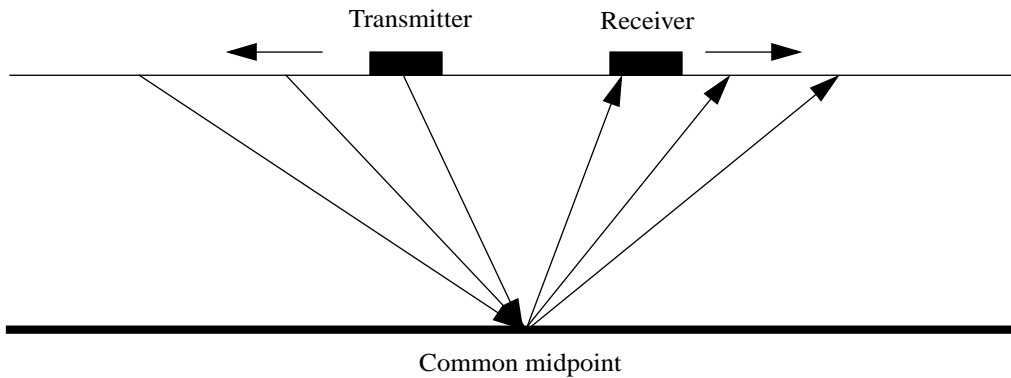
Figure 3. Acquisition geometry for CMP gathers. The common midpoint is the midpoint between the transmitter and receiver. As the two antennas move apart, the common midpoint remains the same, assuming horizontal layering.

the GPR antennas away from each other about their (common) midpoint (figure 3). I started with

100 MHz antennas separated by 0.1 m. I increased the separation 0.1 m by moving each antenna

0.05 m away from the other. The two main direct arrivals are the energy propagating through the

air and through the ground between the antennas. The EM velocity of these linear events is

inversely proportional to the slope of their arrivals. The EM velocity from the reflections are

determined by their normal moveout (NMO), a standard velocity analysis method (Yilmaz, 1987).

The EM velocity change between the silt loam and the underlying asphalt bed should produce a

strong reflection. This reflection will provide the average EM velocity for the silt loam between

the surface and the asphalt.

WOR (Wide offset reflection) geometry

The second method uses the optimal antenna separation (3.5 m) from the CMP surveys to

reliably identify the air wave, the direct ground arrival, and the reflection from the asphalt. These

surveys will be denoted as wide-offset reflection (WOR) profiles, as the offset between the anten-

nas is much wider than is usually used in standard GPR reflection profiles. I start this survey with the transmitter and receiver close together, then one antenna is walked away from the other in small increments until the optimal offset is reached. At this time, both antennas are moved together at a constant step size (figure 4). For this experiment, the antenna were located 1.0 m

Wide offset reflection acquisition
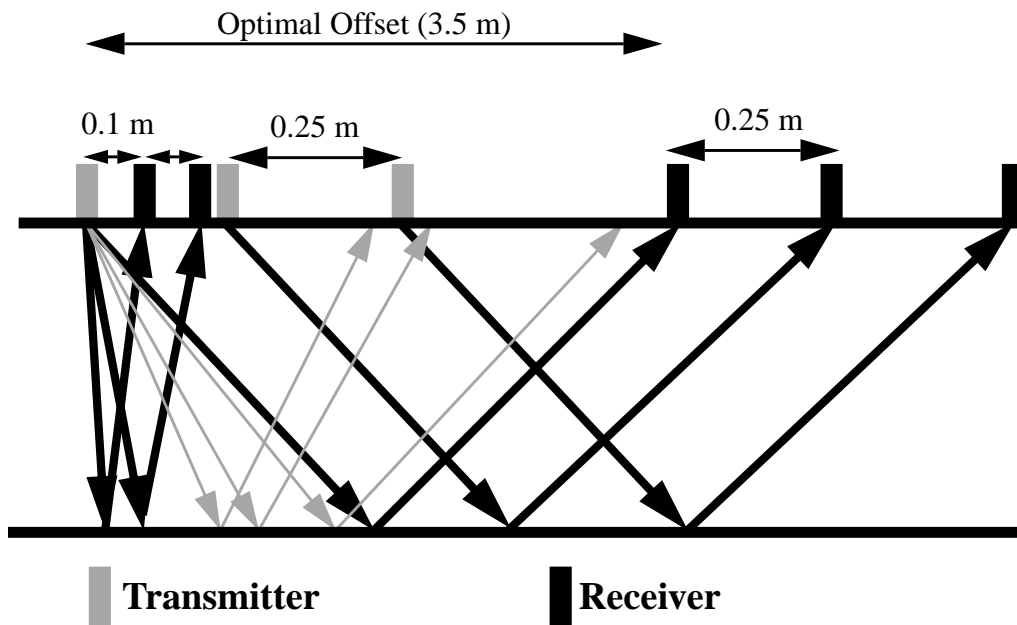
Figure 4. Acquisition geometry for the wide offset profiles. One antenna is held stationary and the other antenna is moved at 0.1 m increments until the optimum offset is obtained. Then the antennas are moved together in 0.25 m increments.

apart, then the receiving antenna only was moved 0.1 m until the antenna separation became 3.5 m. Then both antenna were moved 0.25 m per trace, keeping a constant antenna separation of 3.5 m. This acquisition geometry allows me to identify the ground wave (or other phase) in a pseudo-CMP gather, then follow the event across the WOR profile.

Data and Analysis

I visited the prototype surface barrier site four times to determine the change in soil moisture during the year. I spread the experiments over the year to sample during different seasons. In general at Hanford, Winter is the wet season and Summer is the dry season. Table 1 lists the

Table 1: Geophysical field experiments

Survey Date	Methods
March 9, 2001	GPR and EM-31
May 22, 2001	GPR and EM-31
September 19, 2001	GPR and EM-31
January 9, 2002	GPR and EM-31

acquisition dates and the field methods used.

Figure 5 shows the geometry of the prototype surface barrier and the geophysical surveys. The site is a relatively flat surface covered with rows of sage brush. The outer boundary of the prototype surface barrier is basalt riprap. Grid points are located every 3 m. The origin is located at the first stake (1,1) in the lower, left-hand corner. Irrigation equipment was located at the North end of the site for the March and May surveys.

Two sections of the prototype surface barrier had different water treatment in the past. The northern section underwent a controlled simulated rainfall. The southern section received the ambient rainfall during the year. Water-balance monitoring stations are located along a East-West line at 26 m and 57 m. Stone-tiled access paths are shown in figure 5. The site contains other experimental equipment or access tubes, mostly near the water-balance monitoring stations. The controlled rainfall experiment was completed by the time I started the geophysical experiments.
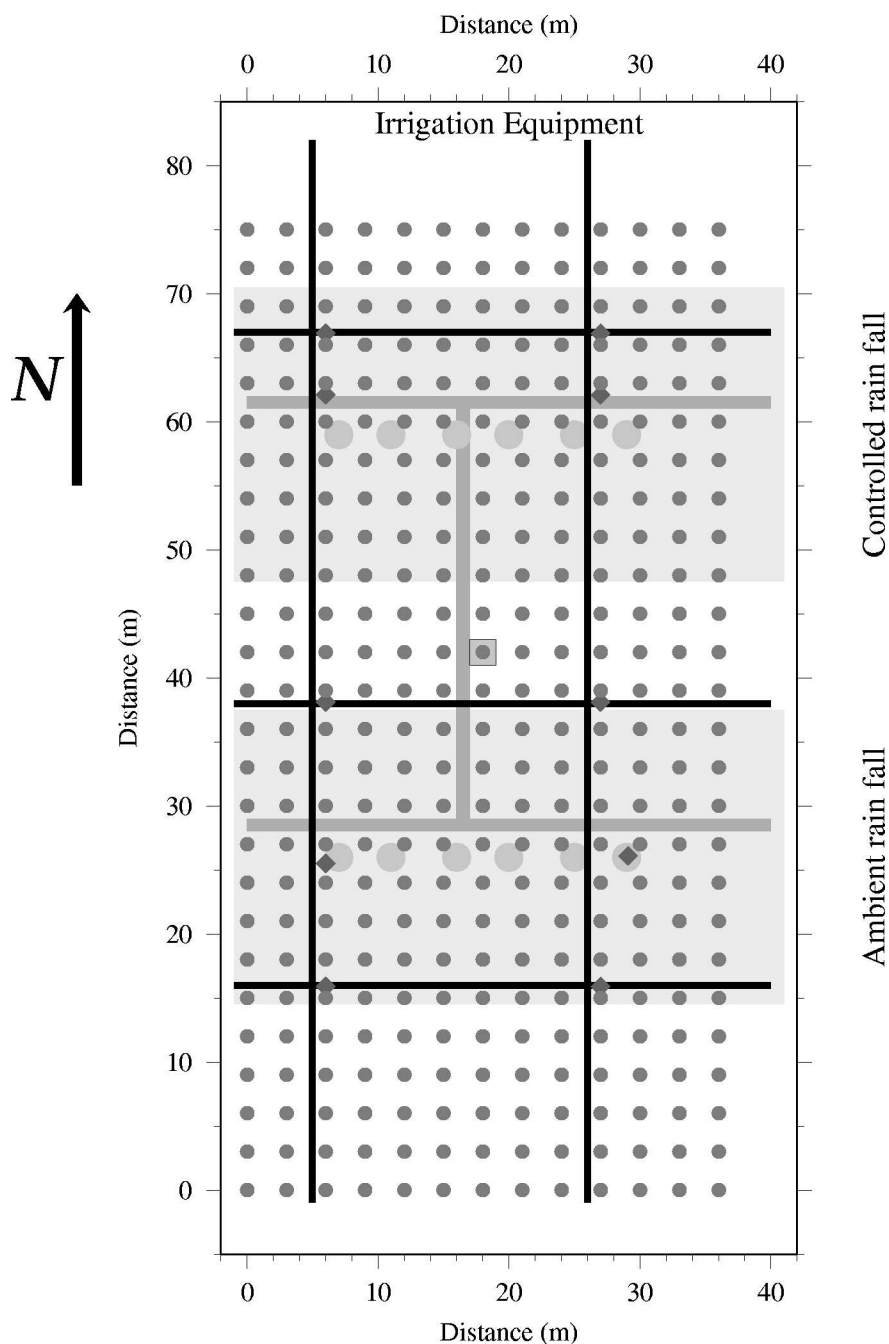
Figure 5. Map showing the CMP locations (dark, grey diamonds), the WOR surveys (black lines), and the EM 31 data collection points (dark, grey circles). The light grey lines are the tiled path ways. The larger, light grey circles are the water-balance monitoring stations and the outlined grey square in the center is the control data logger. The light grey rectangles are the areas monitored for the controlled rainfall experiment.

EM31

I sampled every 3 meters with the EM31-MK2 at each numbered stake. Figure 6. shows
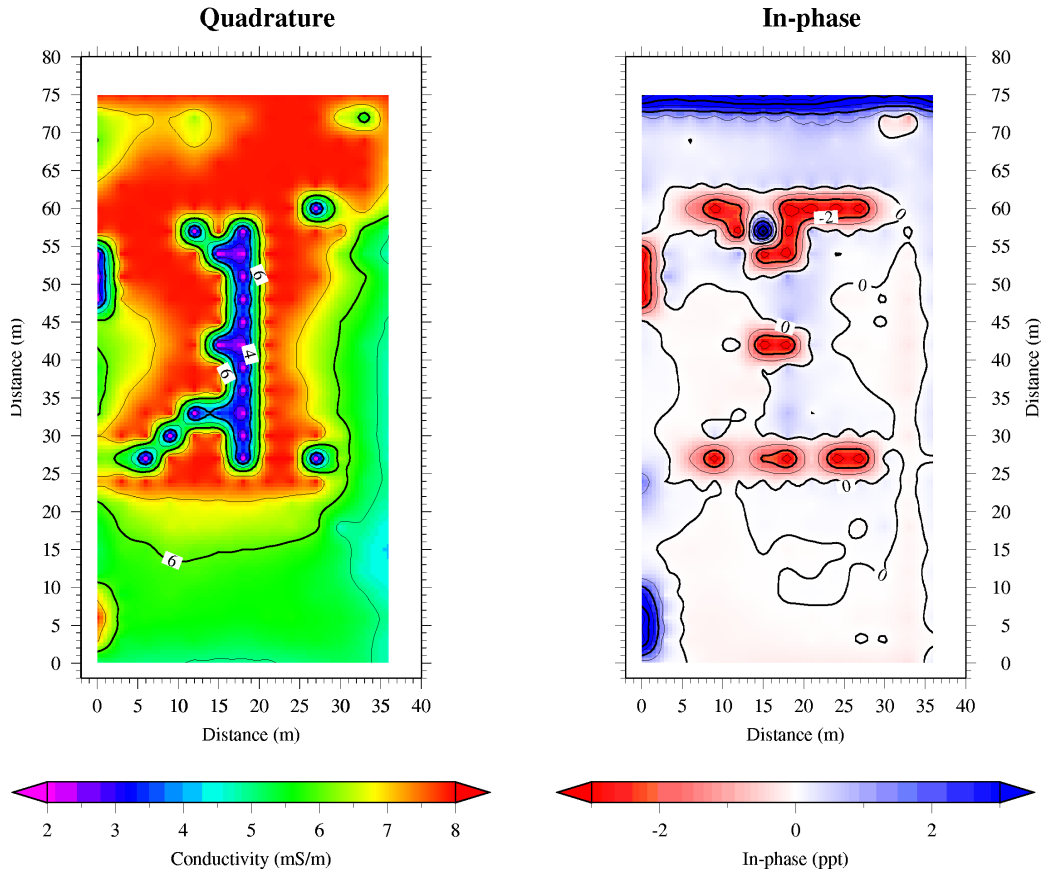
Figure 6. EM31 surveys acquired in March, 2001 with the antenna oriented East-West. The vertical components of the quadrature and in-phase measurements are show.

the quadrature and in-phase components of the March survey The antenna was oriented East-West

in the vertical, coplanar dipole configuration. I also acquired two North-South lines with the

antenna oriented North-South (figure 7). The first North-South survey was along the profile
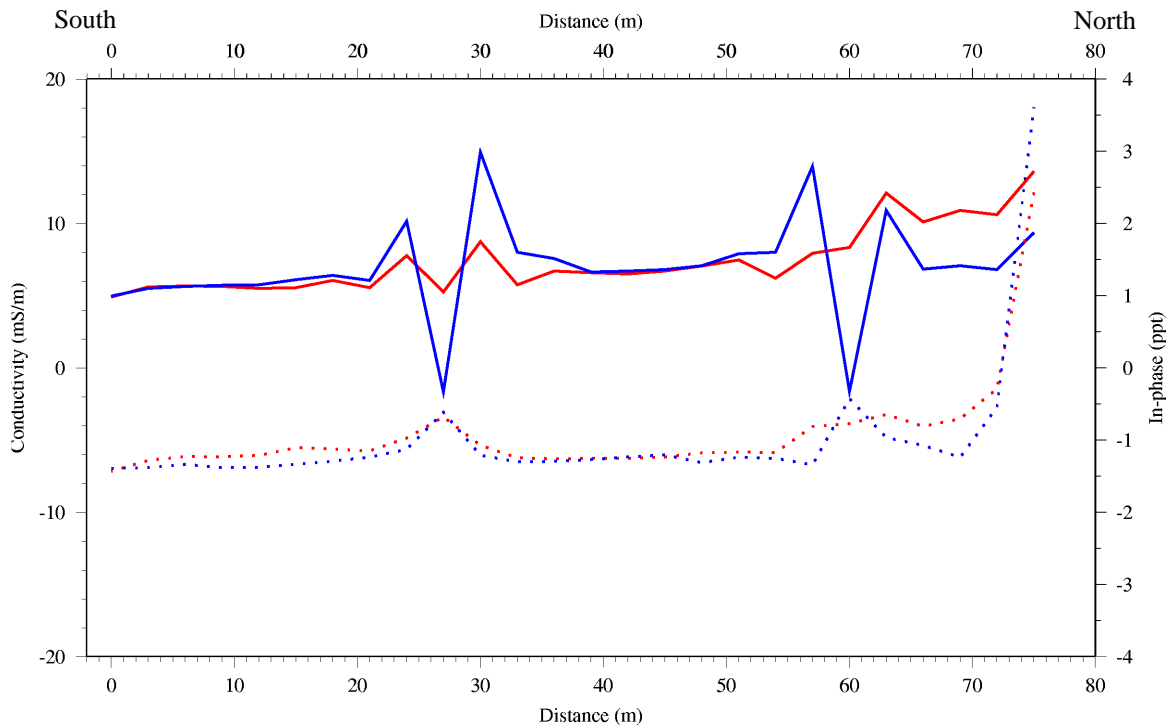
Figure 7. The quadrature and in-phase components of the March North-South surveys. The quadrature component is the solid line; the in-phase component is the dotted line. The NS profile along stake 10 transect is red, the stake 3 m transect is blue.

defined by stakes (10, 1) to (10, 26). The second survey was along the profile defined by stakes (3, 26) to (3, 1). Again, the sampling was at 3 m intervals taken at the stakes along the line. I sampled the current 5 times at each station and recorded the average of those five readings.

The North-South surveys show anomalies corresponding to the water-balance monitoring stations at 26 m NS and 57 m NS. At the North end of the transects, the quadrature and in-phase components separate slightly, with the stake 3 survey having slightly higher values. The higher quadrature values indicate that the Northeast corner has a higher conductivity compared to the Northwest corner. Also the northern-most end values of the in-phase components are much higher

than most of the transect. These high values are probably due to the metal irrigation system at the

North end of the surface barrier.

I compare the changes in the quadrature component of the EM31 data between the four

acquisition dates in Figure 8 and the in-phase components in Figure 9. To facilitate the compari-
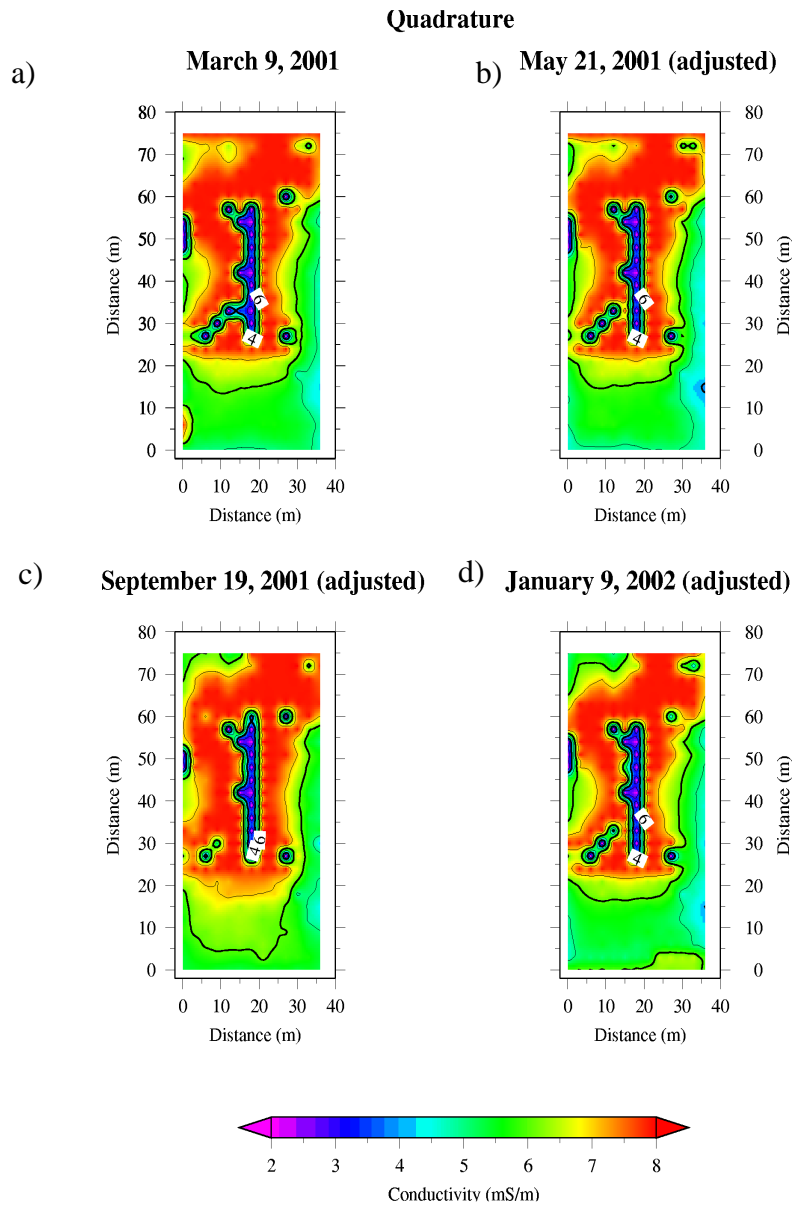
Quadrature

Figure 8. Comparison of quadrature component of EM31 from a) March, b) May, c) September, and January (d). The May, September, and January data were adjusted to have the same average values as the March data.
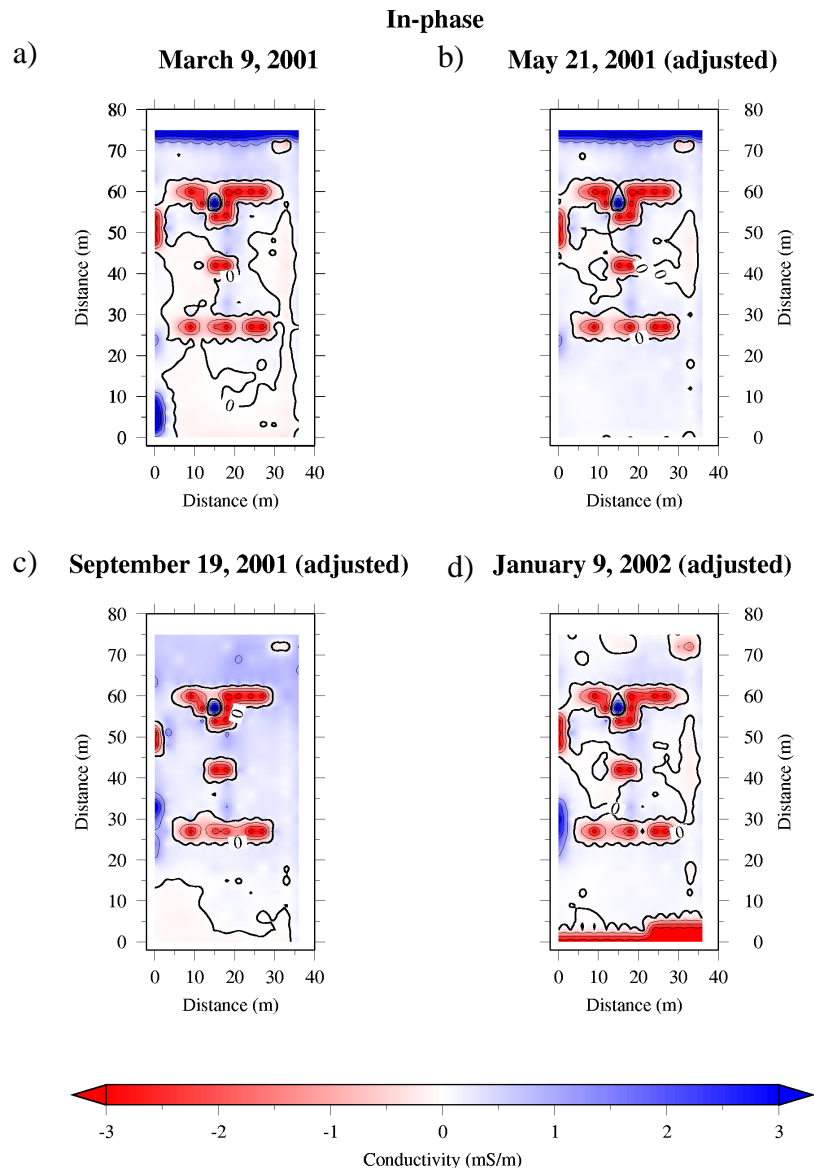
In-phase

Figure 9. Comparison of in-phase component of EM31 from March (a), May (b), September (c) and January (d). The May, September and January data were adjusted to have the same average values as the March data.

son, I have adjusted the May, September, and January surveys. The average of the values in each

component from each month is the same as the average of same component in the March surveys.

In the quadrature component plots, a North-South trending, linear, low conductivity anomaly is

easily observed along 20 m NS. Another, similar anomaly trending in the Southwest direction also

14

appears in the quadrature component data. These anomalies indicate a strongly resistive trend in the prototype surface barrier, possibly related to air-filled conduits.

Another trend in the quadrature component is the decreased conductivity in the southern 20 m of the surface barrier observed in the September survey. The edge of the ambient rainfall plot is at about 15 m EW. In the September data, the transition from red to green is further South than in the other three plots. Otherwise, the plots are remarkably similar and unrevealing.

In the in-phase component plots, strong, East-West trending anomalies are seen at about 27 m NS and 62 m NS. These anomalies correspond to the locations of the water-balance monitoring stations. The in-phase component responds strongly to metal objects. The anomalies are probably due to metal wires and pipes associated with the water-balance monitoring stations and access tubes for related monitoring experiments. The strong anomaly at 18 m EW and 42 n NS coincides with the data control station, a large metallic object.

GPR

<u>CMP surveys</u>

The CMP surveys were acquired with the 100 MHz antennas to determine the subsurface EM velocity and the optimal offset for separating the air and ground waves. The CMPs were centered on the stake locations listed in Table 2. I acquired several CMPs at the beginning of the

Table 2: CMP EM velocity results

CMP location	March Velocity (m/ns)	January Velocity (m/ns)	May Velocity (m/ns)
3, 23.3	0.118	0.110	---
10, 23.3	0.117	0.112	---
10, 23.3	0.115	0.112	---
3, 23.3	0.115	0.110	---

Table 2: CMP EM velocity results

CMP location	March Velocity (m/ns)	January Velocity (m/ns)	May Velocity (m/ns)
3, 21.7	0.116	0.110	---
10, 21.7	0.117	0.115	---
3, 6.33	0.118	0.114	0.142
10, 6.3	0.124	0.117	---
10, 6.3	0.292 (air)	0.299 (air)	---
3, 13.7	0.121	0.114	---
10, 13.7	0.124	0.118	---
10.7, 9.7	0.126	0.125	0.147
3, 9.5	0.120	0.120	---
Average (excl. air)	0.119	0.115	0.1445

March field experiment to determine the optimal offset to collect the WOR data. The optimal offset was based on the time separation of the air and ground waves. I wanted to avoid interference between the two phases so I could accurately pick the ground wave arrival time and amplitude. If the separation is too close, the air wave will interfere with the later arriving ground wave and potentially cause a mispicking of the arrival time and the amplitude. From the March CMPs, I chose an optimal antenna separation of 3.5 m. Although the character of the GPR data changed substantially during the May and September field experiments, fortunately, the 3.5 m offset still allowed picking of the ground wave. Attenuation of the wave's amplitude due to larger separation would have made picking the ground wave unreliable.

Processing of the GPR data consists of a few standard procedures. The data are dewowed to remove low frequency noise due to the electronics in the radar unit. For the CMP analysis, I

bandpass filtered the data between 25 to 200 MHz to increase the signal to noise ratio of the arrivals. The WOR data are unfiltered. For plotting the images, I used an AGC with a 25 ns window.

Figure 10 compares CMPs from locations (10.7, 9.7) for the four acquisition dates. For the March and January data, the ground wave is a strong event. The May data shows a weaker, less extensive ground wave. The May CMP displayed has the best ground wave arrival of May surveys. The September CMPs show weak ground wave arrivals and I could not pick the ground wave for velocity analysis. In the March and January CMPs, the ground wave projected to arrive at 10 m at approximately the same time (~86 ns for March; ~88 ns for January). Thus, their slopes are nearly equal, indicating that the EM velocity of the ground wave is the about same for each date. In May, the projected ground wave arrives at ~75 ns at 10 m antenna separation. This earlier arrival time indicates that the EM velocity is faster in May.

For the March, January, and two May CMPs, I picked the ground wave arrival times where possible and computed the EM velocity using a linear regression. The EM velocity of the arrival is the inverse of the computed slope. Table 2 lists the results from the analysis. The velocities from March and January are nearly the same at each location, with the January velocities consistently slower. At the two locations analyzed from May, the EM velocity is 0.147 m/ns and 0.142 m/ns, significantly faster than the March and January equivalent locations. Although the May velocities are suspect, this simple analysis shows the large change in EM velocity over the year at the prototype surface barrier.

CMP interpretation usually consists of normal moveout (NMO) velocity analysis of the reflections in the data. The reflections in the CMP gathers are corrected for NMO based on many different velocities (Yilmaz, 1987). Those velocities that align the reflections best are indicated by the higher amplitudes in the EM velocity plot (figure 11). The green features at the top of the EM
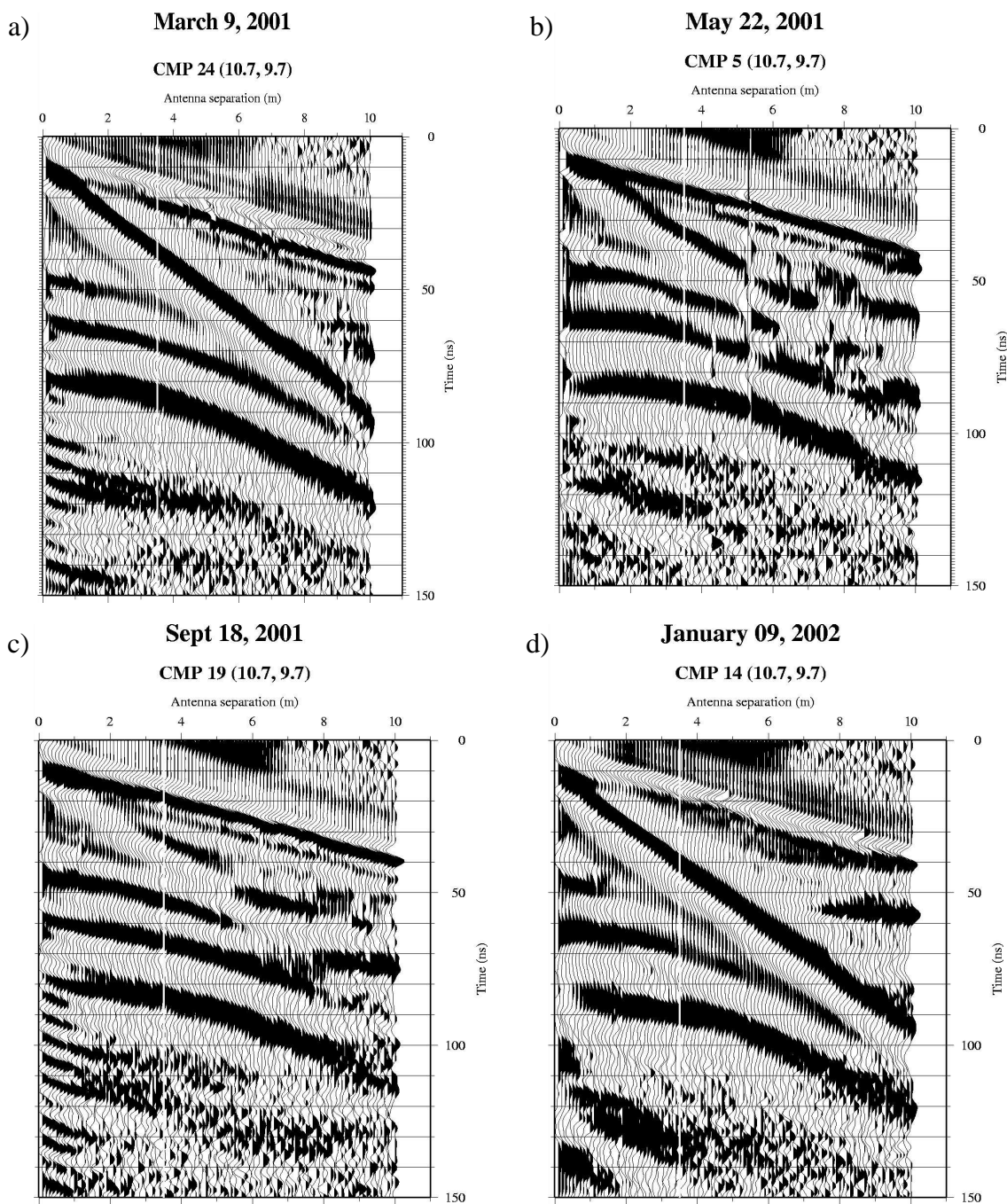
Figure 10. CMP gathers at grid location (10.7, 9.7). The CMPs were acquired in a) March, b) May, c) September, and d) January. Note the changes in the ground wave and reflection character from March to January. The vertical white line in each plot shows the optimal antenna separation.

18

March 9, 2001

Velocity Analysis for CMP 14 (10, 6.3)

a)
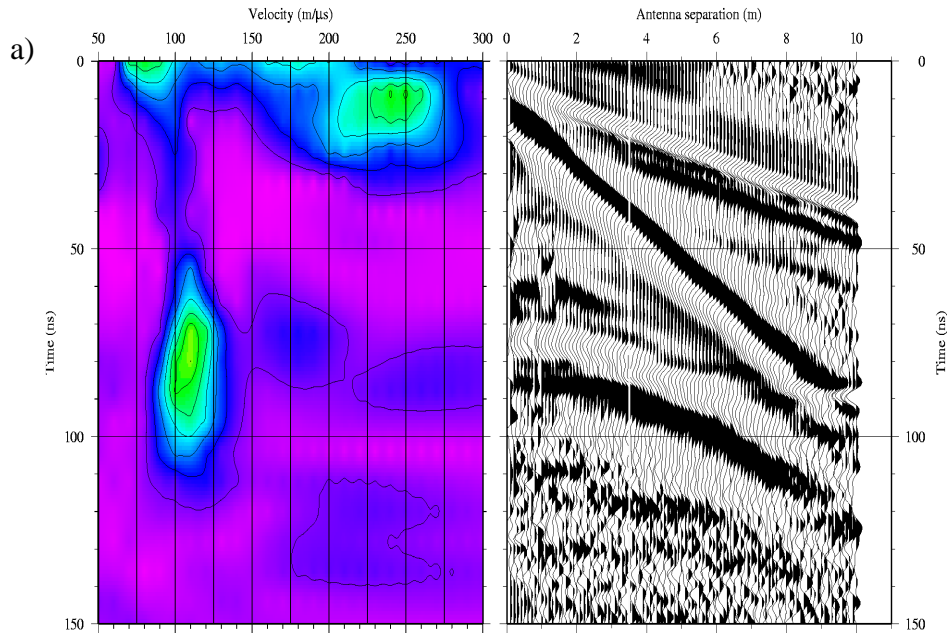
May 22, 2001

Velocity Analysis for CMP 7 (3, 13.7)

b)
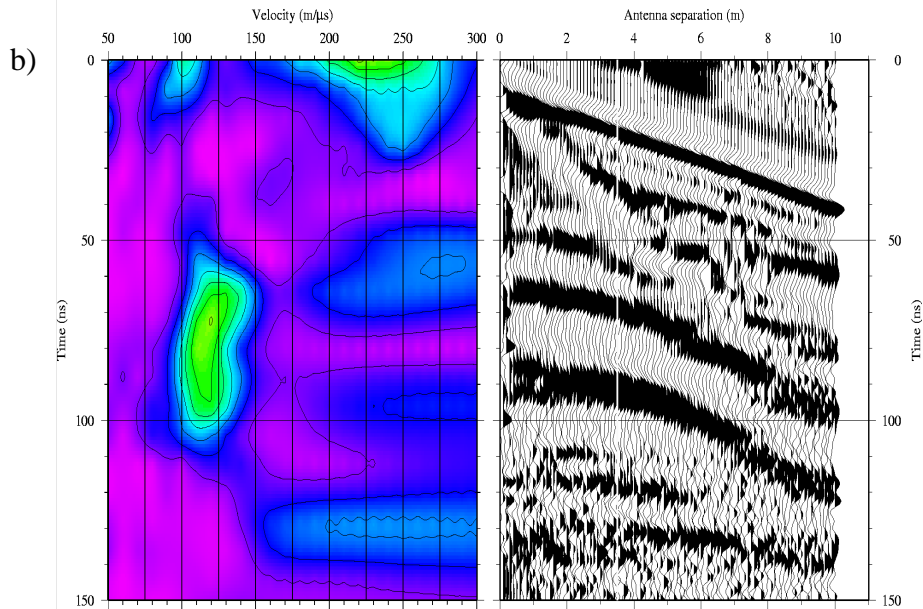
Figure 11. The CMP gather located at (3,13.7) and its velocity analysis acquired during the a) March and b) May experiments. Although the plots are similar, the May velocity is slightly higher.

velocity plot above 40 ns are from the air and ground arrivals. The NMO velocity analysis is only appropriate for reflections. The air and ground waves are direct arrivals, so their velocities are improperly corrected by NMO. The NMO velocity analysis indicates that the reflections have velocities between 0.105 and 0.120 m/ns.

Figure 11 compares the March and May NMO velocity analysis at stake location (3, 13.7). Although the EM velocity plots are similar, the green anomaly between 60 and 100 ns in the May plot is shifted to slightly faster velocities compared to the March plot. Although this EM velocity shift is small, the shift indicates that the material above the reflector has a faster EM velocity in May than in March. This increased EM velocity, although slight, corroborates the EM velocity increase found from the ground wave arrival analysis.

<u>Wide-offset surveys</u>

I acquired five lines of GPR across the field site (Table 3). The three East-West (EW) lines

Table 3: Wide-offset reflection profiles

Line	Direction	Stake system	Tx	Rx	Tx	Rx
1	E-W	Row 23.3	40.5	39.5	4.25	0.75
2	E-W	Row 6.3	40.5	39.5	4	0.5
3	E-W	Row 13.7	40.5	39.5	4	0.5
4	S-N	Col 2.7	0.5	1.5	82	85.5
5	N-S	Col 9.7	82.5	81.5	4	0.5
For lines 1 to 3, the 10 m on the tape corresponds to the 3 column of stakes; the 31 m tape measurement corresponds to the 10 column of stakes. For line 4, 3.9 m on the tape corresponds to row 1 of stakes. For line 5, 4.8 m on the tape corresponds to row 1 of stakes.						

are 40 m long. The two North-South (NS) lines are 80 m long. The GPR data for each survey was acquired with the same parameters, except the stacking change mentioned earlier. The antenna

frequency was 100 MHz. In March, I tested the 200 MHz antennas, but the penetration of the energy was too poor to record large offsets. Each survey was started with a walkaway to help reliably identify the air and ground waves (figure 12).

March - 100 MHz GPR
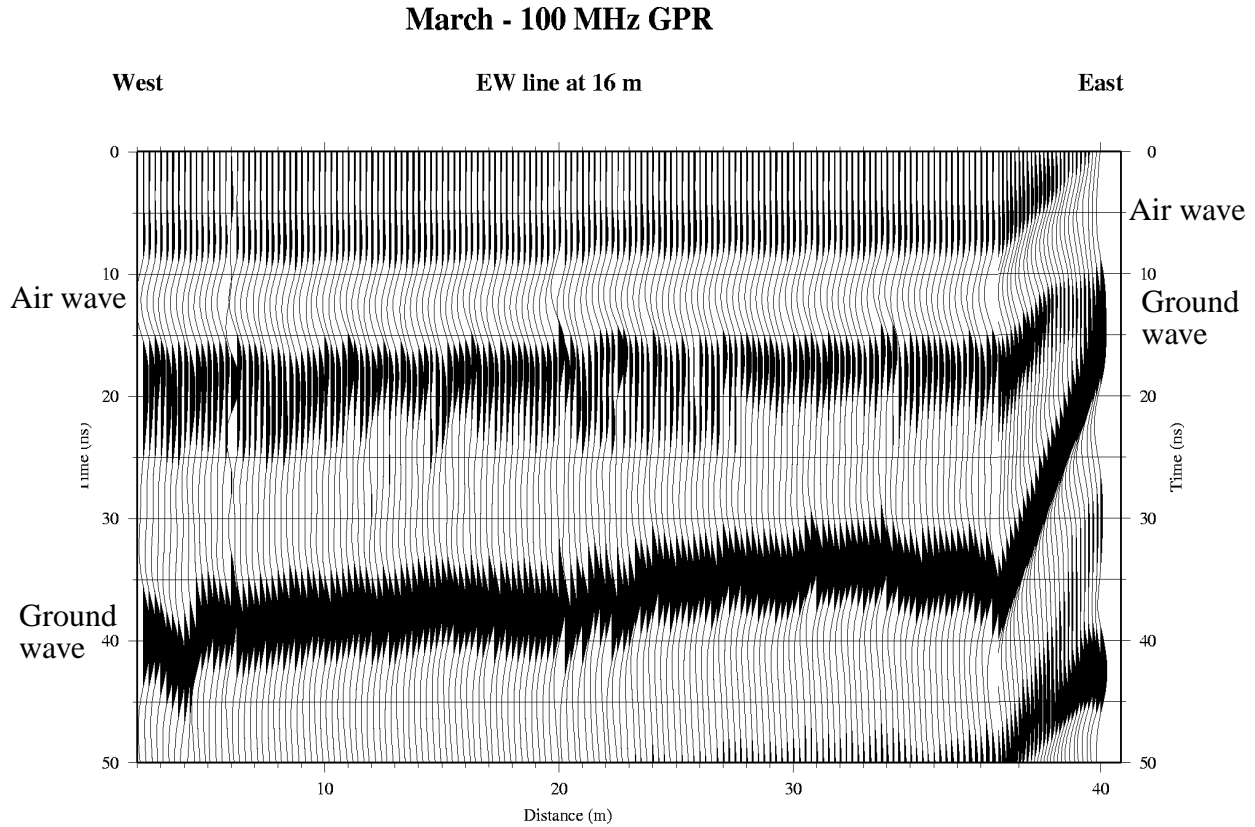
Figure 12. Wide offset reflection profile along East-West profile at 16 m. The walkaway start to the survey is at the West end of the profile. The air and ground wave are labeled. The polarity of the ground wave is reversed from the polarity of the air wave. Note the different length scale between about 39 and 40 m.

An important decision is identifying the air and ground waves. By starting the survey with the walkaway, I can more confidently pick the air and ground waves from the slope and intercept on the time axis of the phases. The air wave also has the opposite polarity from the ground wave (Du and Rummel, 1994). Thus, in the presented data, the air wave has a negative (white) ampli-

tude, whereas the ground wave has a positive (black) amplitude. The opposite polarity further assists in picking the proper phase.

The WOR GPR data analysis consists of picking the arrival times of the air and ground waves at known locations and antenna separations (Figures 13 and 14). In GPR data, the input waveform has a central, large amplitude peak flanked by two smaller peaks. I picked the central peak for my analysis.

Two aspects of the character of the WOR GPR surveys are easily observed in figures 13 and 14. First, the ground wave is strong in the March and January data. The ground wave in the May and September data is more difficult to see and not as coherent. Fortunately, the walkaway start of each survey makes picking the ground wave more reliable. Secondly, the arrival time of the ground wave is about 35 to 40 ns in the March and January data, but is about 30 ns in the May and September data. The earlier ground wave arrival indicates that the EM velocity is faster in May and September compared to March and January.

The GPR data indicates changes in the radar response throughout the year. The most obvious cause in the radar character is changes in the soil moisture content due to a decrease in rain and an increase in evapotranspiration in the Summer months. During the Winter months the rainfall increases and reduced evapotranspiration lessens. To determine changes in soil moisture content, I want to determine the EM velocity of the material sampled by the radar energy. The EM velocity of the air and ground waves is simply:

$$\text{velocity} = \frac{\text{distance}}{\text{time}}. \tag{1}$$

After the EM velocity is determined, the dielectric constant (κ) can be computed from the EM velocity (v):
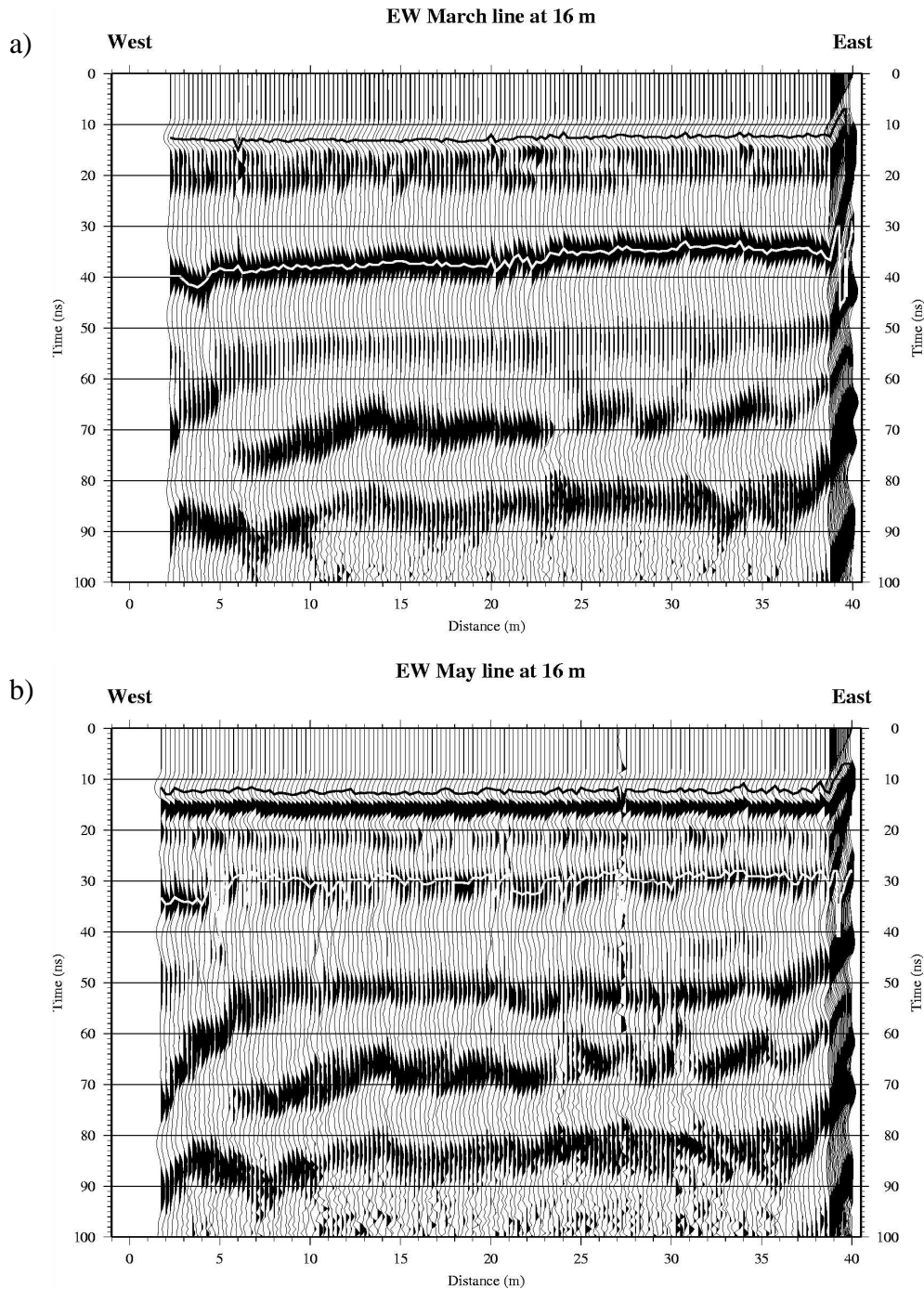
Figure 13. The WOR data from a) March and b) May. Note the weaker ground wave amplitudes and the earlier arrival times in the May profile compared to the March profile. The air wave picks are marked by the black line, the ground wave picks are marked by the white line. Bad picks on the right side of the sections are due to a poorly defined picking window, and are ignored in the interpretation.

EW Sept line at 16 m

West   **East**

EW January line at 16 m

West   **East**
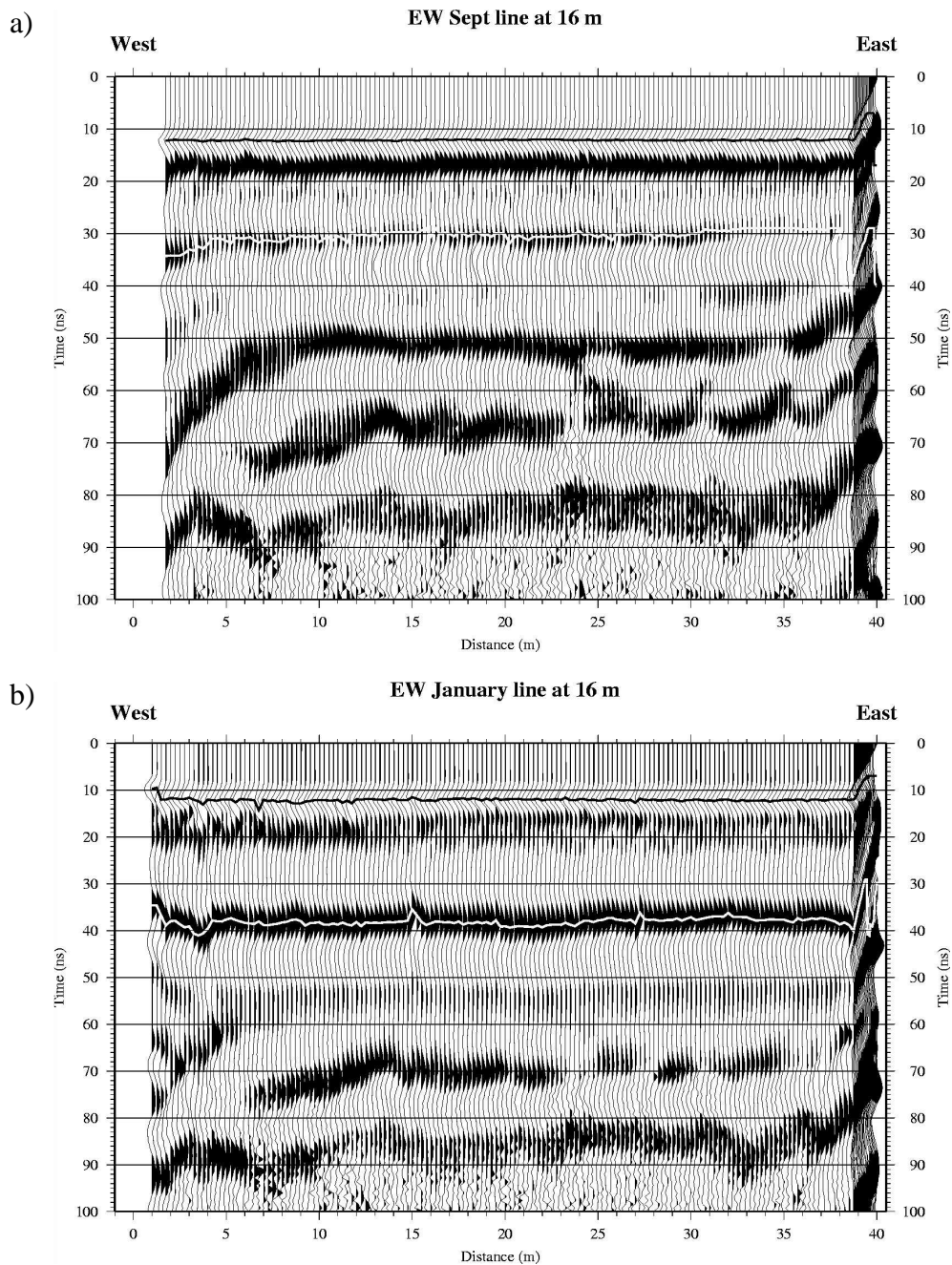
Figure 14. Similar plots to figure 13, showing data from a) September and b) January. Note the weaker ground wave energy and the earlier arrival time of the September profile. The September data is more similar to the data from May. The January data has similar arrival times and amplitudes compared to the March data. Annotations are the same as figure 13.

$$\sqrt{\kappa} = \frac{c}{v} \tag{2}$$

where c is the EM velocity of light (0.3 m/ns).

A more direct way to determine the dielectric constant is to use the arrival times of the air and ground arrivals directly. The square root of the dielectric constant can be computed from the air and ground wave travel time picks (Huisman et al., 2001):

$$\sqrt{\kappa} = \frac{c(t_{ground} - t_{air}) + x}{x} \tag{3}$$

where c is again the EM velocity in air, x is antenna separation (3.5 m), t_{ground} is the arrival time of the ground wave, and t_{air} is the arrival time of the air wave. The ground wave samples a volume of the near surface, providing an average EM velocity for that volume.

The ground wave samples only a portion of the ground between the antennas. Through experiments, Berktold et al. (1998) determined that the ground wave samples below the surface to a depth between one-half to one wavelength. The wavelength (λ) is computed from the frequency (f) and the velocity of the phase:

$$\lambda = \frac{v}{f}. \tag{4}$$

In the GPR data, the antenna frequency is 100 MHz and the EM velocity is about 0.12 m/ns. Thus the sampled depth is about 0.6 to 1.2 m.

In the unsaturated zone, soil moisture content is a critical physical property governing fluid flow. Recall that EM velocity is strongly dependent on the amount of water present in the soil. The dielectric constant of water is 80, whereas air is 1. In dry soils, the dielectric constants have a narrow range of about 3 to 10. Because of the large difference in dielectric constant,

25

changes in EM velocity are strongly tied to changes in the water content. Soil moisture content can be derived from the EM velocity of the soil. Mixing laws based on the amounts of the constituent materials present are used to convert EM velocity to soil moisture content (Knoll et al., 1995). The dielectric constants can also be converted to soil moisture content using established petrophysical relationships such as Topp's equation (Topp et al., 1980):

$$\theta = -5.3x10^{-2} + 2.92x10^{-2}\kappa - 5.5x10^{-4}\kappa^2 + 4.3x10^{-6}\kappa^3 \tag{5}$$

where θ is the water content.

The changes in EM velocity of the ground wave along the EW16 profile acquired in March are shown in figure 15. Figure 15 also shows the derived soil moisture content values. To

March 9, 2001
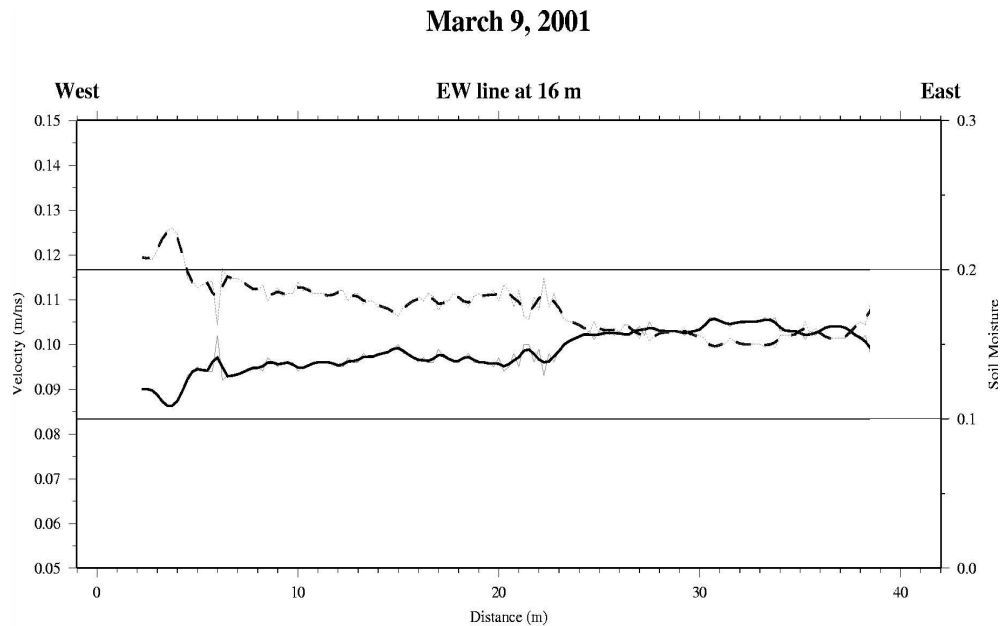
Figure 15. Velocity (solid line) and soil moisture (dashed line) from EW line 16 in March. The velocity is computed using Huisman et al.'s equation (eqn 4) and the soil moisture is derived from the velocity using Topp's equation (eqn 3). The thin gray lines are the actual values. The heavy black lines are a smoothed version of the values using a 5-point running average.

more easily see the trends in the values, I applied a 5-point running average to smooth the values. The smoothed version and the calculated values are plotted in figure 15. The EM velocity changes are derived from eqn (3). The soil moisture estimates are derived from Topp's equation (eqn 4). The EM velocity increases from about 0.085 m/ns on the West to about 0.105 m/ns on the eastern side of the prototype surface barrier. The soil moisture decreases from 0.22 in the West to 0.15 in the East.

The changes in EM velocity along EW16 over the course of the experiment are shown in figure 16. The EM velocity increases significantly in May, then remains about the same in Sep-
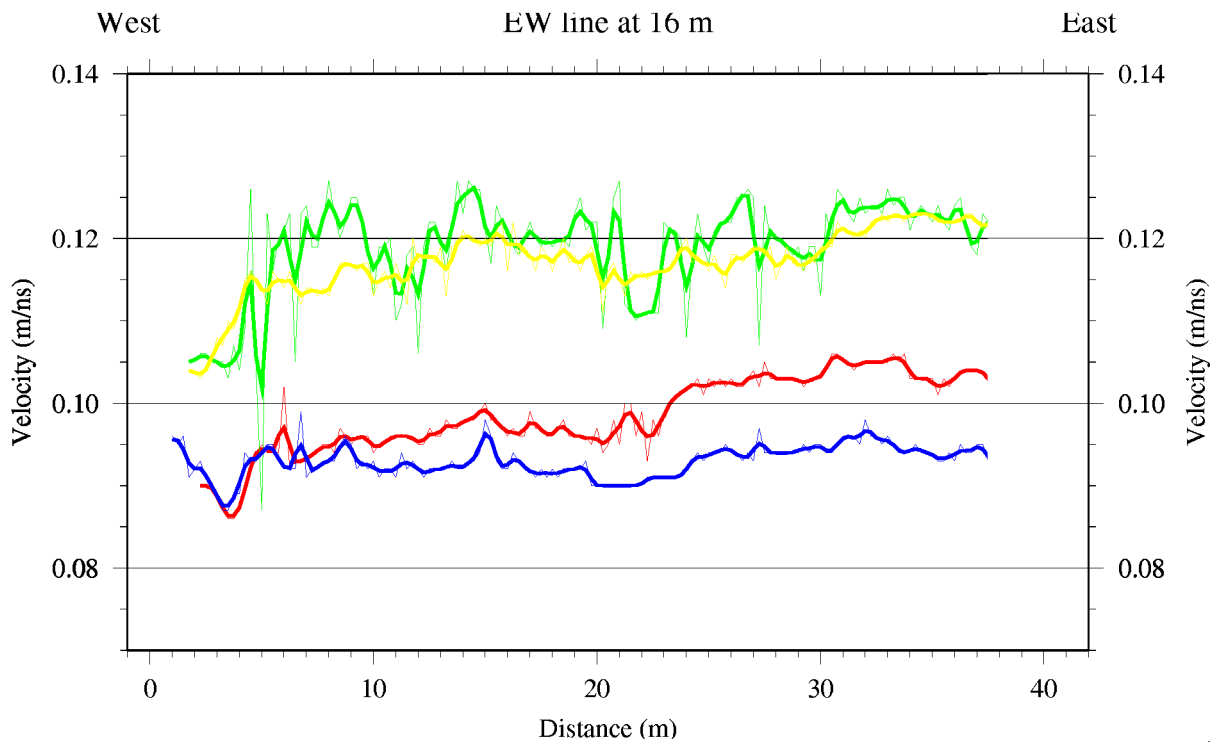
Figure 16. Velocity changes along EW16 from March to January. March -- red; May -- green; September -- yellow; January -- blue.

tember. The EM velocity then decreased in the January data. The EM velocity is lowest during

January. Similarly, the soil moisture decreases in May, then remains about the same in September, then increases in January to wetter values than in March (figure 17).
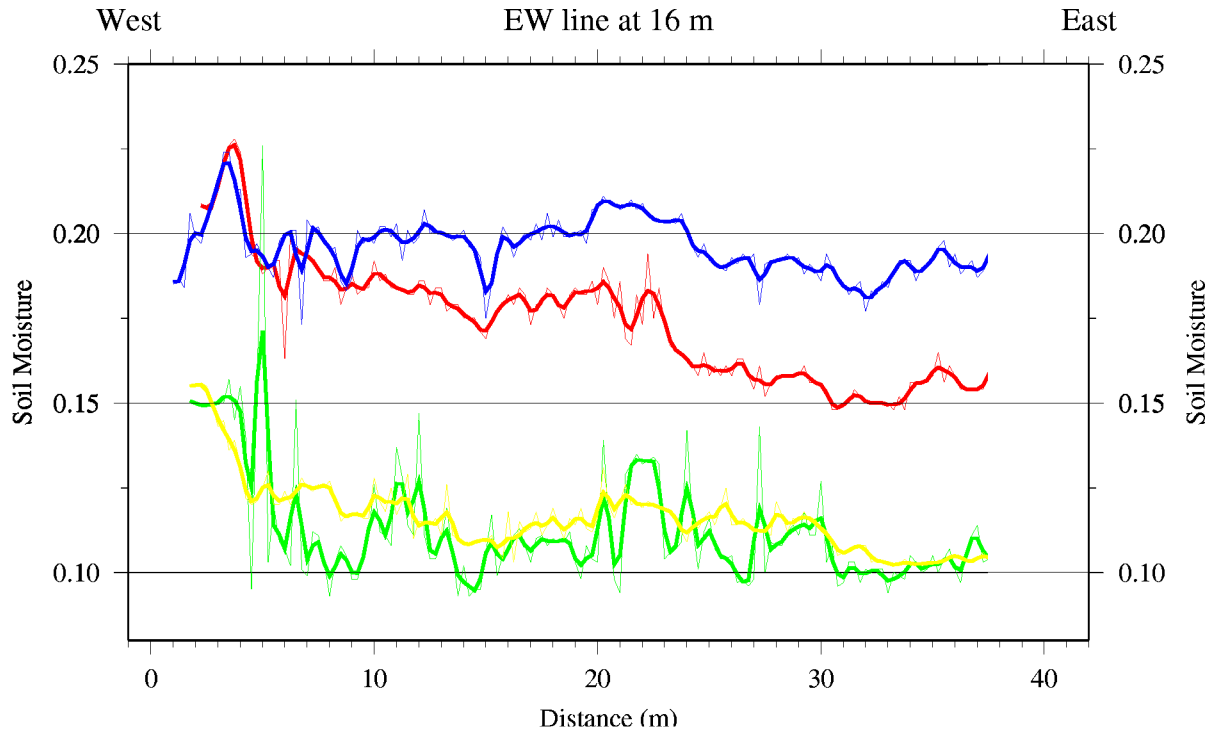
Figure 17. Soil moisture changes over time along line EW16. March -- red; May -- green; September -- yellow; January -- blue.

I am also investigating the effects of soil moisture on amplitude. I have picked the largest absolute value amplitude in a window corresponding to the arrival time of the phase. I use the absolute value because of the polarity change between the phases. Figure 18 shows the amplitude of the ground wave arrival. To compare the amplitudes from different acquisition times, I have normalized the ground wave amplitudes by dividing by the air wave amplitude. I use the maximum of the absolute value of the amplitude, because the two phases have different polarities. The amplitudes from the GPR are influenced by many, variable factors, including the battery strength and coupling between the antenna and the ground. I assume that the electromagnetic properties of

28
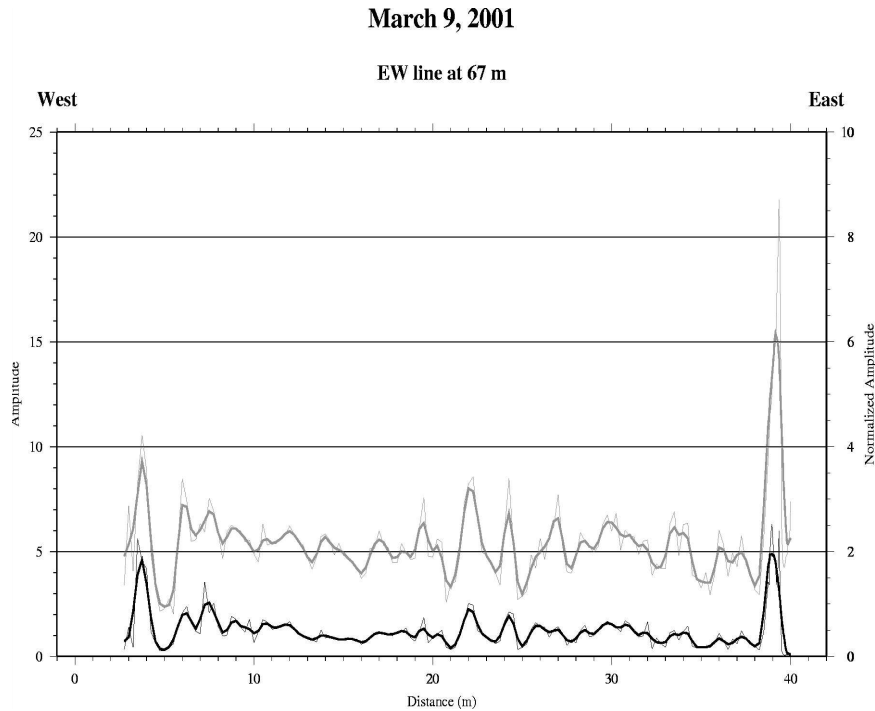
Figure 18. Amplitude of ground wave (gray) for EW line at 67 m acquired during march. The black line is the normalized amplitude (abs(Ground/Air)). The left and right axes are different.

the air wave do not change between surveys. Thus, the amplitude measured by the air wave includes these variable factors, but not changes in EM properties. By normalizing with the air wave, I can remove coupling effects and other instrument fluctuations in the ground wave amplitudes between the surveys. Thus, the changes in amplitude are due to changes in the soil properties.

Du and Rummel (1994) note that the amplitude of the ground wave increases as $\sqrt{k}$ relative to that of the air wave. Thus, the ground wave is better observed in wet soils compared to dry soils. Reviewing figures 13 and 14, the ground wave amplitudes weaken in the drier, Spring and Summer months relative to the Winter months. Figure 19 shows that the normalized amplitudes along EW line 67. The largest amplitudes are in March and January, the smallest are in May and

West EW line at 67 m East
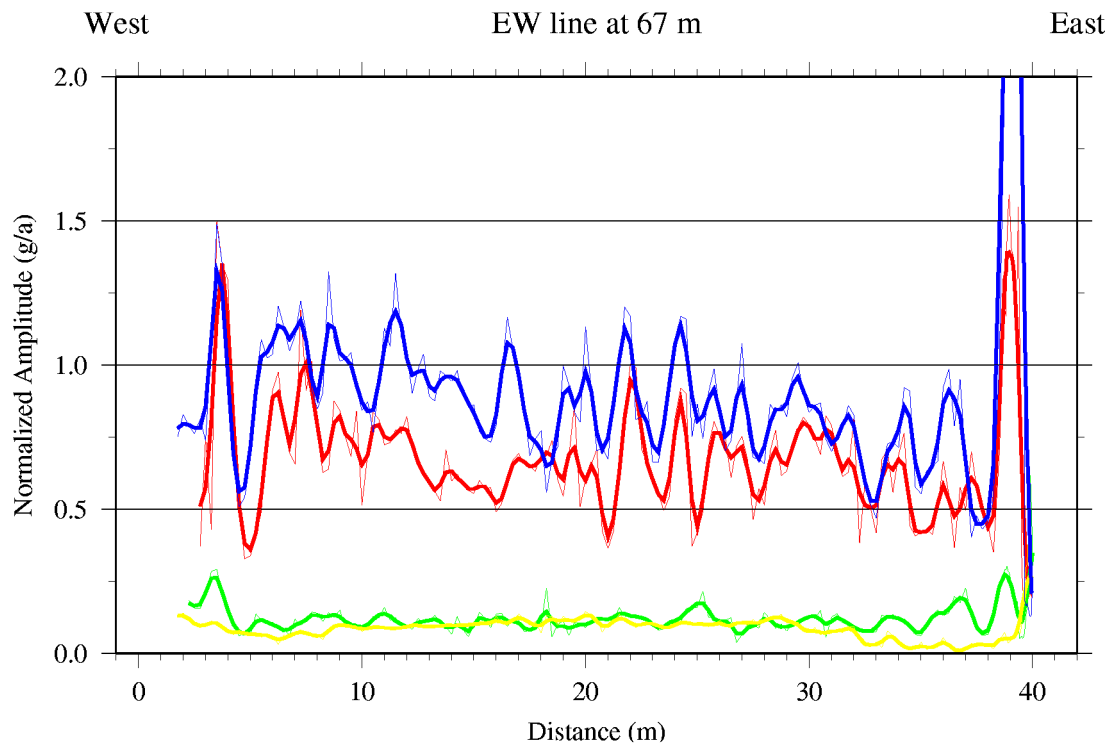
Figure 19. Normalized amplitude changes over time along EW line 67. March --
red; May -- green; September -- yellow; January -- blue.

September. These amplitude changes indicate that the soil moisture decreases during the Spring

and Summer months and is replenished in the Winter months.

From figure 19, I would predict that the soil moisture during January was highest. The

moisture content decreases slightly in March, then by May, the water content decreased substan-

tially. The amount of moisture remained relatively constant between May and September, then

increases during the Fall. These changes probably reflect the changes in rainfall throughout the

year.

Conclusions

GPR has great potential to observe changes in soil moisture content over time. Changes in

the GPR character are easily observed over the course of the experiment. These changes corre-

spond to EM velocity changes indicating that the soil moisture changes over time in an expected way. Amplitude analysis indicates that the soil moisture changes in a manner similar to the EM velocity analysis.

The EM31 conductivity data lacks the resolution necessary to observe the soil moisture changes. At the prototype surface barrier, the soil moisture changes occur in the upper 2.5 meters. EM31 samples deeper into the barrier. This deeper penetration may cause the poor spatial resolution of the EM31 data.

GPR proved successful at imaging changes in soil moisture over the year. Because the EM velocity changes are large between the dry and wet season, GPR soil moisture estimates will probably be reliable. Using GPR to determine soil moisture content has many advantages over traditional methods: 1) the cost and speed of data acquisition is relatively inexpensive; 2) the large spatial sampling density provides greater coverage; and 3) the method is non-intrusive. GPR is a promising technique to determine the 3-dimensional distribution of the soil moisture content in the subsurface.

References

200-BP-1 Prototype barrier treatability test report, US Department of Energy, DOE/RL-99-11, Rev. 0, 1999.

Berktold, A., K. G. Wollny, and H. Alstetter, Subsurface moisture determination with the ground wave of GPR, Proceedings from GPR '98, 7th International Conference, May 27-30, 675-680, 1998.

Chanzy, A., A. Tarussov, A. Judge, and F. Bonn, Soil water content determination using a digital ground-penetrating radar, Soil Science Society of America Journal, 60, 1318-1326, 1996.

Charlton, M., Small scale soil-moisture variability estimated using ground penetrating radar, SPIE Proceedings Series, 4084, 798-804, 2000.

Curtis, J. O., Moisture effects on the dielectric properties of soils, IEEE Transactions on Geoscience and Remote Sensing, 39, 125-128, 2001.

Davis, J.B., N. R. Kitchen, K. A. Sudduth, and S. T. Drummond, Using electromagnetic induction to characterize soils, Better Crops with Plant Food, #4, Reference 323075/98116, 1997.

Du, S., and P. Rummel, Reconnaissance studies of moisture in the subsurface with GPR, Proceedings of the fifth international conference on Ground Penetrating Radar, GPR '94, 1241-1248, 1994.

Greaves, R. J., D. P. Lesmes, and M. N. Toksoz, Velocity variations and water content estimates from multi-offset, ground-penetrating radar, Geophysics, 61, 683-695, 1996.

Grote, K., S. Hubbard, and Y. Rubin, GPR monitoring of volumetric water content in soils applied to highway construction and maintenance, The Leading Edge, 482-485; 504, 2002.

Hubbard, S., K. Grote, and Y. Rubin, Mapping the volumetric soil water content of a California vineyard using high-frequency GPR ground wave data, The Leading Edge, 21, 552-559, 2002.

Huisman, J. A., C. Sperl, W. Bouten, J. M. Verstraten, Soil water content measurements at different scales: accuracy of time domain reflectometry and ground-penetrating radar, Journal of Hydrology, 245, 48-58, 2001.

Knoll, M. R. Knight, and E. Brown, Can accurate estimates of permeability be obtained from measurements of dielectric properties?, SAGEEP95, 1995.

Lesmes, D. P., R. J. Herbstzuber, D. Wertz, Terrain permittivity mapping: GPR measurements of near-surface soil moisture, SAGEEP99, 575-582, 1999.

McNeill, J. D., Electrical conductivity of soils and rocks, Geonics Limited, Technical note TN-5, 22 p.,1980a.

McNeill, J. D., Electromagnetic terrain conductivity measurement at low induction numbers, Geonics Limited, Technical note TN-6, 15 p.,1980b.

Sheets, D. K., and J. M. H. Hendrickx, Noninvasive soil water content measurement using electromagnetic induction, Water Resources Research, 31, 2401-2409, 1995.

Topp, G. C., J. L. Davis, and A. P. Annan, Electromagnetic determination of soil water content: Measurements in coaxial transmission lines, Water Resources Research, 16, 574-582, 1980.

van Genuchten, M. T., A closed-form equation for predicting the hydraulic conductivity of unsaturated soils, Soil Science Society of America Journal, 44, 892-898, 1980.

van Overmeeren, R. A., S. V. Sariowan, J. C. Gehrels, Ground penetrating radar for determining volumetric soil water content: Results of comparative measurements at two test sites, Journal of Hydrology, 197, 316-338, 1997.

Weiler, W. K., T. S. Steenhuis, J. Boll, and K.-J. S. Kung, Comparison of ground penetrating radar and time-domain reflectometry as soil water sensors, Soil Science Society of America Journal, 62, 1237-1239, 1998.

Yilmaz, O., Seismic Data Processing, Society of Exploration Geophysicists, Investigations in Geophysics, v. 2, S. M. Doherty, (ed.), p. 526, 1987.